Detection of the lensing galaxy for the double QSO HE 1104−1805 ⋆

M. Remy, J.-F. Claeskens[1], J. Surdej[2],

Institut d'Astrophysique, Université de Liège, Avenue de Cointe 5, B–4000 Liège, Belgium

J. Hjorth,

Nordic Institute for Theoretical Physics, Blegdamsvej 17, DK–2100 Copenhagen Ø, Denmark

S. Refsdal, O. Wucknitz,

Hamburg Observatory, Gojenbergsweg 112, D–21029 Hamburg, Germany

A. N. Sørensen,

Copenhagen University Observatory, Niels Bohr Institute for Astronomy, Physics and Geophysics, Juliane Maries Vej 30, DK–2100 Copenhagen Ø, Denmark

F. Grundahl

Dominion Astrophysical Observatory, Herzberg Institute of Astrophysics, National Research Council of Canada, 5071 W. Saanich Road, Victoria, BC. V8X 4M6, Canada

---

Abstract

High angular resolution ground-based direct imaging (V, R, I_c) of the double QSO HE 1104−1805 has been obtained with the NOT and NTT telescopes. Analysis of these data led to the first detection of the lensing galaxy. Direct imaging of HE 1104−1805 has subsequently been carried out with the Planetary Camera (WFPC2) through the F555W (nearly Johnson V) and F814W (nearly Kron-Cousins I_c) filters onboard HST. These images confirm the presence of the deflector between the two lensed quasar components (A & B). Direct imaging of this system in the near infrared (IR) at 2.2 μm (K'), with IRAC-2b at the Cassegrain focus of the ESO/MPI 2.2 m telescope, indicates that the additional component is indeed a very red extended object with magnitude $K \approx 16.5$. We present deconvolutions of the HST and IR images using the 2-channel PLUCY method. From the HST observations, we also report very accurate relative positions and brightnesses of

Preprint submitted to Elsevier Science *2 February 1998*

the QSO components. By comparison between the ground-based and the HST observations, from February–March 1994 to November 1995, we possibly detect the fading of component A by ~ 0.3 magnitudes in the optical and a corresponding fading of B by about half this value. The observed monotonic decrease of the magnitude difference between B and A as a function of wavelength is consistent with a partial amplification of the A component by microlensing. Evolutionary models for galaxies show that, in order to produce the observed colour indices $V - I_{\rm c} > 2$ and $4 < I_{\rm c} - K < 4.5$, the galaxy is likely to be of elliptical type with a redshift $0.95 < z < 1.4$. This range is consistent with the redshift $z = 1.32$ measured from the absorption lines of metallic species in the spectra of the quasar components. However, other values for the redshift of the lens inside this range cannot be excluded. This galaxy would presently be among the most distant known gravitational lenses. Several theoretical models are found to fit the observations. The simplest one is a singular isothermal sphere (SIS) lens immersed in an external shear with $\gamma = 0.123$. The derived mass-to-light ratio ($11\, h_{50}\, \mathcal{M}_{\odot}/\mathcal{L}_{\odot}$) for the galaxy is large but does not imply an excess of dark matter with respect to other well known lensing galaxies.

Keywords: — gravitational lensing — quasars: individual: HE 1104−1805 — techniques: image processing

---

1 Introduction

Since the discovery in 1979 of the first gravitational mirage produced by the bending of light rays from a distant quasar by a massive foreground galaxy (Walsh et al. 1979), gravitational lensing has proved to be a valuable tool for cosmology and astrophysics. This research has led, among many other results, to tight constraints on the value of the Hubble constant from the measurement of time delays, to a better understanding of the properties of distant deflecting galaxies and to interesting studies of microlensing effects induced by dark compact objects over small regions of the background quasar. We here present some new results based on direct imaging of the doubly

[⋆] Based on observations made with the NASA/ESA Hubble Space Telescope (HST), obtained at the Space Telescope Science Institute, which is operated by the Association of Universities for Research in Astronomy, Inc., under NASA contract NAS5-26555, with the Nordic Optical Telescope (NOT), operated on the island of La Palma jointly by Denmark, Finland, Iceland, Norway, and Sweden, in the Spanish Observatorio del Roque de los Muchachos of the Instituto de Astrofísica de Canarias, with the European Southern Observatory/Max Planck Institute (ESO/MPI) 2.2 m telescope and with the ESO 3.5 m New Technology Telescope (NTT) in La Silla, Chile.

[1] Aspirant du FNRS, Belgium.

[2] Directeur de Recherches du FNRS, Belgium.

imaged quasar HE 1104−1805.

HE 1104−1805 was discovered to be a good gravitational mirage candidate with a redshift $z = 2.303$ by Wisotzki et al. (1993, 1995). From the observed variability, these authors report the signature of both intrinsic variations and changes due to microlensing. They stress the importance of direct observations of the lensing galaxy in order to model the macro-lensing configuration in detail. Prominent absorption lines in the spectrum of this quasar indicate the possible presence of galaxies at redshifts $z = 1.6616$ (damped Lyα and many metallic species) and $z = 1.320$ (SiIV, SiII, CIV, MgII, ...) along the line-of-sight (see Smette et al. 1995 for an exhaustive list of several systems with the identification of absorption lines).

On the basis of observations obtained with the NOT in February and March 1994, Grundahl, Hjorth and Sørensen (1995) were the first to report the presence of a very red object between A and B at a distance of $1''.15$ from A with $I_c \sim 20.6$, the probable lensing galaxy. This detection was subsequently confirmed on the basis of one single ESO NTT 3.5 m frame also obtained in February 1994. A summary of these ground-based NTT and NOT observations is presented in Section 2 together with a more detailed photometric analysis.

Following this first set of observations, we have included HE 1104−1805 as a priority target in the framework of a study of gravitational lensing with HST. The corresponding direct imaging, data reduction and analysis are described in Section 3.

Large infrared to optical colour indices are expected for lensing galaxies at large redshift. The detectability of such relatively faint galaxies is then easier in the near IR than in the optical. We have therefore carried out ground-based observations of this object at 2.2 μm under good seeing conditions. The data were obtained at ESO in January 1997 in the framework of pilot studies of gravitational lensing in the near IR and their analysis is presented in Section 4.

The final photometry of the two quasar components is compared between the different data sets and the science results of this comparison are presented in Section 5.

A discussion based on the observed photometric properties of the lensing galaxy forms the content of Section 6. Modeling of the lens configuration consistent with the above observations is discussed in Section 7. The main conclusions of this study are summarised in the last Section. Throughout this paper, we assume that the Universe is described by an Einstein-de Sitter model ($\Omega_0 = 1$ and $\Lambda_0 = 0$). Unless stated otherwise, the Hubble constant H_0 is assumed to be 50 km s^{-1} Mpc^{-1}.

2 Ground-based optical direct imaging of HE 1104−1805

On February 12, 1994, a direct image of 300s was obtained with SUSI at the NTT through the I_c filter under a seeing with Full Width at Half Maximum (FWHM) of 0.″9. A simultaneous subtraction of two scaled point-like components from this frame leads to the detection of significant residuals between HE 1104−1805 A and B, confirming the likely presence of the deflector (G) previously reported by Grundahl et al. (1995) on the basis of the NOT data. The magnitude of the quasar components and of the lensing galaxy derived on the basis of the NTT frame is presented in Section 5 (Table 3).

The NOT data (15 I_c images, in total 8100s; 6 R images, in total 2800s; 1 V image, 180s) were obtained on February 23 and 24, 1994 and on March 20 and 30, 1994 under good seeing conditions (0.″6–0.″7). The deep image resulting from the co-addition of the I_c frames is presented in Figure 1. Photometry of the stars in the field is also given in Section 5 (Table 2).

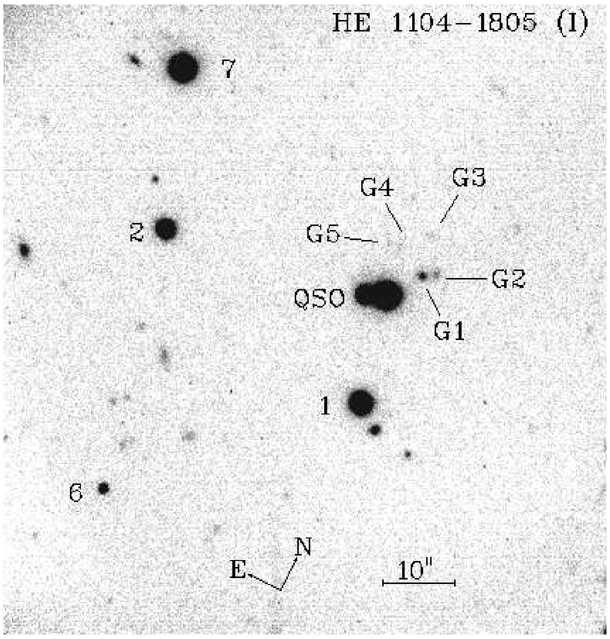

Fig. 1. Deep NOT I_c image (8100s) of the field around HE 1104−1805 A and B (QSO). The 3-σ detection limit for point sources is 22.7 mag (FWHM=0.″7). Several extended objects are conspicuous. In the immediate vicinity (10″) of the quasar, we detect 5 galaxies; its brightest member G1 was already reported by Wisotzki et al. (1993). Star identifications come from Wisotzki et al. (1995); stars 6 and 7 are new.

Photometry in the R and I_c bands of the NOT images was derived using the DAOPHOTII/ALLSTAR/ALLFRAME package (Stetson 1987, 1994). For each image, we derived a PSF using stars 1 and 2. ALLFRAME was then fed with the derived positional transformations between the images. Using

ALLFRAME for these reductions allows one to derive the R photometry of the galaxy G despite the fact that it is too faint to be detected on the individual R images. ALLFRAME then uses the positional information from the I_c images on which the lensing galaxy G is detected for estimates of its magnitudes.

The ALLFRAME photometry provides marginal evidence for variation in the 15 NOT I_c images in which the magnitude difference B−A changed from 1.703 ± 0.006 in February 1994 to 1.688 ± 0.003 in March 1994. Since an object as bright as the lensing galaxy may not affect by more than 1.4 % the I_c flux of the A component, the possible contamination by the light from the galaxy is ought to be much less than 0.01 mag.

3 HST direct imaging of HE 1104−1805

One HST orbit was allocated to the planetary camera (PC1) observations of HE 1104−1805 (proposal ID 5958), which took place on November 23, 1995. Based on the photometry already reported for this system, our strategy was to obtain 2 exposures of 100s with the F555W filter (nearly Johnson V), 4 exposures of 200s with F814W (nearly Kron-Cousins I_c) and two additional 100s exposures with F814W. We chose the ADC channel with 14 e^-/ADU gain. Offsets by $\approx \pm 0\farcs92$ and $\pm 0\farcs67$ along the columns and rows of the PC1, corresponding to approximately ± 20.25 pixels in Y and 14.75 pixels in X, were introduced between each of four consecutive exposures. The aim was to optimally dither the QSO images in order to detect more easily faint structures at small angular scales. Indeed, as it is well known, the pixels of the PC1 undersample the point spread function of the HST by a factor of about two. Thus WFPC2 does not recover a substantial fraction of the spatial information that exists in the focal plane of the instrument. However, this information is not completely lost as it can be recovered by dithering or sub-stepping the position of the CCD chips by non-integral pixel amounts (Fruchter 1997). With the choice of the above offset values (integers plus quarters of pixels in X and Y), we were able to optimally dither the QSO images and also to easily remove the hot pixels and cosmic rays (Freudling 1995).

Composite F555W and F814W images of the quasar, made after proper re-centering and co-addition of the single PC1 frames are shown in the upper panels of Figure 2. On the composite F814W image, we immediately notice a diffuse object between A and B, identified as the lensing galaxy G. This object is not detected on the composite F555W image. The projected position of its peak is displaced from A by about one third of the angular separation between A and B. Accurate positions of B and of the peak intensity of G with respect to A are given in Table 1. Note that the galaxy is not exactly co-aligned with A and B.

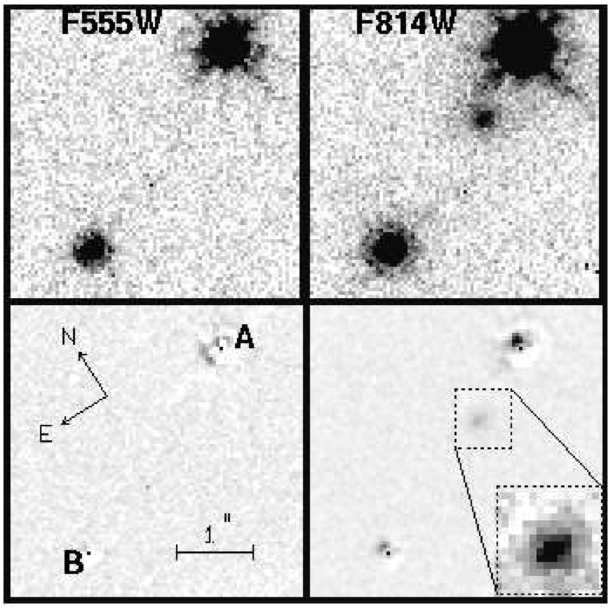

Fig. 2. Composite F555W (upper left panel) and F814W (upper right panel) PC1 CCD frames of HE 1104−1805. From the F555W data (integration time of 200s), we only observe the two quasar components; the complex structure of the HST PSF is well seen. From the F814W observations (integration time of 1000s), we detect the lensing galaxy G near the brightest component A. The lower panels correspond to the results of 2-channel PLUCY deconvolutions (MIDAS version) using appropriate simulated TinyTim PSFs. Most of the flux from the QSO images peaks within a single pixel; the level of the residuals which are left over is at most $\pm 0.2\%$ of the peak flux. An inset (zoomed by a factor 2) illustrates the deconvolved image of the galaxy with low cuts in the lookup table. North is rotated counterclockwise by 31.°99 from the vertical.

A set of approximately 100 simulated PSFs were computed by means of the TinyTim program v4.2 (Krist and Hook 1996, Krist 1997) for different values of the focus (Zernicke parameter Z4) and of the jitter of the telescope. These numerical PSFs were then fitted to the images of HE 1104−1805 A and B with an automatic procedure described in Østensen et al. (1997). Optimal values for the Z4 and the "jitter" parameters were then derived for each individual CCD frame. Due to the breathing of the telescope, departures of up to 7 μm were found for the focus (Z4) during the series of the F814W observations. Selecting the optimal Z4 and jitter parameters, the relevant PSF was built with an oversampling factor of 10. An iterative procedure was used to address the problem of fitting the HST PSF peak after proper re-centering and re-sampling of the final TinyTim PSF. Finally, the 2-channel PLUCY application program (MIDAS version by Hook and Lucy 1994, with 100 internal iterations to ensure quasi-convergence) was fed with these PSFs to deconvolve each single CCD frame of HE 1104−1805. The combined results of those deconvolutions are presented for the F555W and F814W filters in the lower panels of Figure 2. The main aim of the deconvolution process is to search for the presence

	$\alpha('')$	$\delta('')$	θ ($''$)
A	0.000	0.000	0.000
B	2.905 (0.01)	-1.331 (0.003)	3.195 (0.01)
G	0.965 (0.03)	-0.523 (0.05)	1.10 (0.03)

Table 1
HST relative positions (α, δ) and angular separations θ of HE 1104−1805 B and of the lensing galaxy G with respect to A. The values are derived from free position fitting of three components on the F814W data (see Section 3). A de Vaucouleurs model is used for the galaxy. Standard-deviations are given in parentheses.

of additional point-like components located at a projected distance of several pixels from the positions of the bright point-like components. No new component has been detected. The very faint residuals of the deconvolution seen in the vicinity of A and B are easily interpreted as artefacts due to the noise and undersampling of the PSF core.

We also decomposed all images of HE 1104−1805 A and B using two point-like components (their positions and brightnesses being the only free parameters). We observe insignificant residuals around the point-like components. Comparison with the corresponding residuals from star 1 clearly indicates that the residuals near A and B are due to an effect in the real PSF not accounted for by TinyTim. The presence of these artefacts unfortunately prevents the detection of point sources fainter than the A component by approximately 5 mag and located at $< 0\farcs13$ from the PSF center. Adopting a scale of $0\farcs04553$ (pixel)$^{-1}$ for the PC1 detector, we derive an average angular separation of $3\farcs195 \pm 0\farcs01$ between HE 1104−1805 A and B.

For the case of the F814W data, a de Vaucouleurs (a) profile with ellipse-shaped isophotes has also been fitted to the galaxy. Due to the moderate S/N in the galaxy, a gaussian (b) or exponential (c) profile fits this object as well. Some simulations have then been performed to address the accuracy on the derived effective radius or effective surface brightness of the de Vaucouleurs profile. There is essentially no way to determine accurate values for these parameters on the basis of our F814W data: the galaxy does not appear to be sufficiently extended and/or bright. After subtraction of any of the optimal models (a, b or c), no significant residuals are left for the galaxy. The angular separation between A and the galaxy is derived to be $1\farcs10 \pm 0\farcs03$ (see Table 1 for accurate relative positions of the quasar components and of the galaxy).

At larger angular separation from the quasar, we very marginally detect the G1–2 galaxies (Figure 1). They appear on the 200s F814W frames but not on the other HST frames. The difficulty of detecting such faint extended objects is not surprising given the large focal ratio differences between the HST and the used ground-based telescopes.

We follow the standard HST photometric procedure of integrating the flux of point sources in the classical $0\farcs5$ aperture (Whitmore 1997). The values of the PHOTFLAM were taken from the keyword appearing in the header of the frames. We derived the individual magnitudes of HE 1104−1805 A, B and star 1 in the Johnson V and Kron-Cousins I_c systems (see Tables 2 and 3) from the F555W and F814W in-flight magnitudes, following the method outlined in Holtzmann et al. (1995), where colour corrections, CTE corrections, and zero-point corrections from the STMag to Vega photometric systems are introduced. The magnitude differences between the quasar components are measured to be $\Delta V = 1.74 \pm 0.01$ and $\Delta I_c = 1.60 \pm 0.01$.

The number of counts in F814W for the galaxy is derived in two steps. First, we fit the composite I_c image with two numerical PSFs for A and B and a de Vaucouleurs model for the galaxy. The galaxy counts are derived, not from the best model itself, but integrating the flux after subtraction of the two optimal numerical PSFs from the frame. In this way, the galaxy counts are found to be independent of the galaxy model used in the first step. The integrations have been performed using CCD aperture photometry with radii of $0\farcs95$ and $1\farcs35$. The multi-colour galaxy photometry is discussed in Section 6.

4 IRAC-2b observations

HE 1104−1805 was also imaged at the Cassegrain focus of the ESO/MPI 2.2 m telescope using the IRAC-2b camera and a K' (2.2 μm) filter on January 19, 1997. To limit the sky background, the observational technique was to add 3 frames of 30s each taken at a fixed position on the sky and then to dither the telescope by several seconds of arc and take another set of 3 exposures. We finally got 18 mean frames of the object, each with a total integration time of 90s. The average seeing of the set of 18 frames is $\approx 0\farcs9$ (FWHM).

Stars 1 and 2 (see Figure 1) appear to be well suited for the determination of an accurate PSF. To check the validity of this PSF, it was fitted to all point-like objects and this test was successful for all but one: the very red star 7 appears to be superimposed on an extended object.

Each of the individual frames is of moderate S/N and a direct analysis of these frames is dubious. Using the positions of all unsaturated stars, a direct co-addition S_1 of the 18 frames was computed; another co-addition S_2 was obtained after pixel replication by a factor 2 in both directions.

We successfully modeled the S_1 and S_2 images of HE 1104−1805 with the help of two numerical PSFs for the quasar components and a de Vaucouleurs model convolved with the PSF for the galaxy. We have derived the optimal effective radius and effective surface brightness with a method similar to the one used for the HST F814W observations (see Section 3). The fit of S_1 or S_2 with such a model led to insignificant residuals for a large range of the de Vaucouleurs parameters. As for the HST data, the residuals are also insignificant when we use gaussian or exponential models. However, derivations of the effective radius and surface brightness have been performed on a limited set of simulated data to test their stability. Variations up to a factor 2.5 in effective radius and 0.5 in surface brightness have already been observed when changing the noise seed of the simulated frames. The limitation of the method is also induced by the convolution process. Determination of the real de Vaucouleurs parameters will only be possible when higher angular resolution and S/N images of the galaxy become available.

The angular separation between A and B is derived to be $3\farcs17 \pm 0\farcs03$, a value fully consistent with the more accurate HST value. In order to reduce the number of free parameters, we have finally fixed the relative positions of the configuration using the accurate F814W positions given in Table 1 and the observed relative orientations between the frames. This new fitting leads to statistically negligible residuals (the derived magnitudes are given in Table 3). The IR counts for the galaxy were obtained by integration inside an aperture after removal of 2 scaled PSFs for A and B as in Section 3 for the determination of the F814W galaxy counts. Note that because the optical and IR observations of HE 1104−1805 were not taken simultaneously, the quasar variability (see Section 5) may possibly affect the derived optical to IR colour indices for its components.

Deconvolution with the PLUCY 2-channel algorithm of the high resolution S_2 image is presented in Figure 3. It reveals an elongated object for the deconvolved galaxy for which the peak intensity location is consistent with the HST position. The magnitude of the galaxy directly derived from the PLUCY deconvolution is identical to the value derived from the PSF subtraction method using the $1\farcs35$ aperture ($\Delta m \leq 0.01$ mag).

After deconvolution, the galaxy seems to be less extended on the HST I_c data (FWHM $\approx 0\farcs2$) than on the near IR ground-based images (FWHM of $\sim 0\farcs7$ in α and $\sim 0\farcs4$ in δ). However, some tests on similar simulated extended objects reveal a dependency of the derived sizes on the S/N and seeing in the image. These tests show that, in the case of the IR ground-based images, our determinations of the FWHM for the deconvolved image of the galaxy can easily be overestimated by a factor 2.

The galaxies at larger angular separation from the quasar are not detected in K'. This last result indicates that they are not as red as the lensing galaxy and/or that their redshifts are smaller.

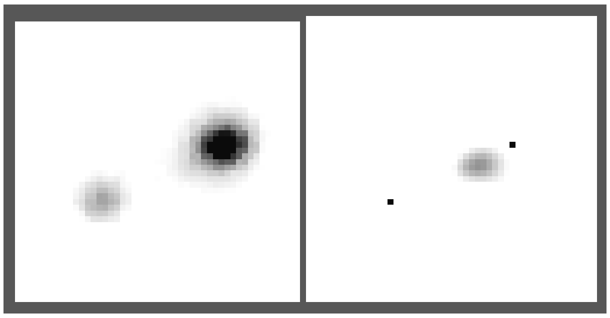

Fig. 3. Composite K' high angular resolution frame of HE 1104−1805 (S_2, FWHM=0.″9) and its deconvolved image. The right panel corresponds to the results of PLUCY 2-channel deconvolution using an appropriate numerical PSF. By comparison with the HST relative positions for B and the same reference star 1, we derive the scaling factor of the IR array to be 0.″2751 per original pixel, and a clockwise rotation angle 31.°57 with respect to Figure 2. North is hence approximately up and East to the left.

5 Multi-colour photometry and quasar variability

The final photometry is given in Table 2 for the stars and in Table 3 for the quasar components and the galaxy. The optical zero-points were first computed independently for the NOT, NTT and HST data. Since the derived I_c magnitudes of star 1 are, within the error bars, mutually compatible and because its colours are not too different from those of the quasar, the more precise HST zero-point was adopted for all the V and I_c data, leading to minor corrections for the derived NTT and NOT magnitudes.

Variability of the quasar, already detected by means of the first calibration, is confirmed by the final cross-calibrated magnitudes. From February–March 1994 to November 1995, a decrease of the flux by 0.28 ± 0.06 mag in V and 0.26 ± 0.05 mag in I_c is observed for the A component, whereas a variation by 0.13 ± 0.06 mag in V and 0.16 ± 0.05 mag in I_c is seen for B. As previously discussed, such a variability could not be accounted for by a contamination of the light from the galaxy.

The monotonic decrease of B−A as a function of increasing wavelength (1.89–1.74 in V, 1.81 in R, 1.69–1.60 in I_c and 1.30 in K) appears well bounded by the lower value (1.12) reported by Wisotzki et al. (1993) for the difference of magnitude derived from the emission line flux ratio between A and B. It is also fully compatible with the magnitude difference between B and A of 1.85 in the B band reported by Wisotzki et al. (1995). The effect of microlensing is most prominent for small sources, leading to chromatic effects if an extended source is not of uniform colour (as we expect for the continuum source of a QSO). These different values of B−A are probably induced in part by apparently chromatic microlensing effects on the continuum of A. Our observations thus

star	V	R	I_c	K
1	17.62	17.21	16.70	15.57
2	18.38	17.92	17.39	16.51
6	20.41	20.66	20.13	—
7	18.74	17.79	16.03	14.04

Table 2

Photometry of the stars in the field around HE 1104−1805. The I_c magnitudes were first calibrated independently for the NOT (± 0.15 mag), NTT (± 0.15 mag) and (star 1 only) HST (± 0.05 mag) data and yielded maximum differences of 0.08 mag, well within the estimated uncertainties. The HST zero-point was then adopted for all the final V and I_c magnitudes (± 0.05 mag) and the NOT zero-point (± 0.10 mag) for the final R magnitude. The zero-point for the 2.2 μm data, in the K standard system, is estimated to be 20.79 ± 0.1 for fluxes expressed in counts s^{-1}.

	NOT Feb–Mar 1994			NTT Feb 1994	HST Nov 1995		ESO/MPI Jan 1997
Object	V	R	I_c	I_c	V	I_c	K
A	16.46	16.39	16.07	16.09	16.74	16.33	14.90
B	18.35	18.20	17.77	17.78	18.48	17.93	16.20
G(0″.95)	—	22.46	20.83	20.50	>23	20.93	16.93
G(1″.35)					>23	20.88	16.44
B−A	1.89	1.81	1.70	1.69	1.74	1.60	1.30
1−A	1.16	0.82	0.63	0.61	0.88	0.37	0.67

Table 3

Photometry of the A & B components of HE 1104−1805 and of the lensing galaxy G. The magnitudes are determined using the same zero-points as those in Table 2. For the point-like objects, the main contribution to the errors comes from the photometric calibration. The accuracy on the relative magnitudes between star 1 and the QSO components is 0.01–0.02 mag in R and I_c and 0.03 mag in V. Radii of the aperture used to evaluate the magnitudes of the galaxy are indicated in parentheses. The error bars for the galaxy magnitudes are 0.2 mag in R, 0.04 mag in I_c (NOT), 0.3 mag in I_c (NTT), 0.1 mag in I_c (HST) and 0.2 mag in K.

support the interpretation of spectral differences and variability in terms of microlensing effects first proposed by Wisotzki et al. (1993, 1995).

6 Discussion of the lens photometry

We present in Figure 4 the $V - I_c$ and $I_c - K$ colour indices of galaxies computed as a function of redshift up to $z = 3$, with and without evolution (Fioc and Rocca-Volmerange 1997). This figure also illustrates the importance of evolutionary correction on the computed $I_c - K$ index for galaxies with redshifts larger than 0.5. In the remainder, because of the great influence of evolution on colour indices for galaxies at large redshift, we will only consider models in which this evolution is taken into account. For $z < 1.5$, the curves do not depend much on the adopted cosmological model. For the case of spiral or irregular type galaxies with evolution, it is difficult to account for an $I_c - K$ colour index larger than 3.5. The observed colour index $4 < I_c - K < 4.5$ is therefore expected to correspond to an elliptical galaxy with $0.95 < z < 1.40$. The upper limit $V - I_c > 2$ implies $0.4 < z < 1.6$ for an evolved elliptical. Using the NOT R magnitude, we deduce a $R - K \sim 5.5$ colour index, slightly smaller than the value $R - K = 5.85$ measured for the elliptical galaxy 53W091 ($z = 1.55$, $R = 24.6$) by Dunlop et al. (1996). As the expected colour index $R - I_c$ is not as sensitive as the above indices to the morphological type or redshift of the galaxy, its value $R - I_c = 1.6 \pm 0.2$, derived from the NOT data, does not efficiently improve the constraint on the morphological type or redshift of the lens.

If we assume that the galaxy redshift corresponds to one of the absorption line systems, the observed indices are then more consistent with the redshift of the metallic absorption line system at $z = 1.32$ and much less with the damped Lyα system at $z = 1.66$. Given that no damped Lyα absorption line has ever been securely identified with an elliptical (see Le Brun et al. 1997), it is quite likely that the intervening galaxy is at redshift $z = 1.32$. Indeed an examination of the FOS spectra observed for HE 1104−1805 by Lopez et al. (1998) confirms that the Lyα line is strong but not damped in the absorption system at $z = 1.32$. Given the extended ionized gas detected by Caon et al. (1995) and also by Plana and Boulesteix (1996), for a large fraction of local early-type galaxies, there is no apparent contradiction with an elliptical deflector at $z = 1.32$ being also responsible for the observed metallic absorption line system. The relatively less strong absorption by metallic species at $z = 1.32$ in the spectrum of B with respect to A supports the idea of a decrease in the gas column density as a function of the distance from the center of G. HE 1104−1805 G would presently be the most distant known galaxy inducing a QSO gravitational mirage. The $z = 1.66$ damped Lyα absorption is possibly produced by gas associated with a foreground galaxy disk. On the basis of the derived $I_c - K$ colour index, the system at $z = 0.728$ (Smette et al. 1995) is excluded as a candidate for the redshift of the lens. However, there remains the possibility that the lens is not associated with any of the detected absorption line systems (Smette et al. 1995). Hence our identification of the lensing galaxy redshift should still be regarded as an open issue.

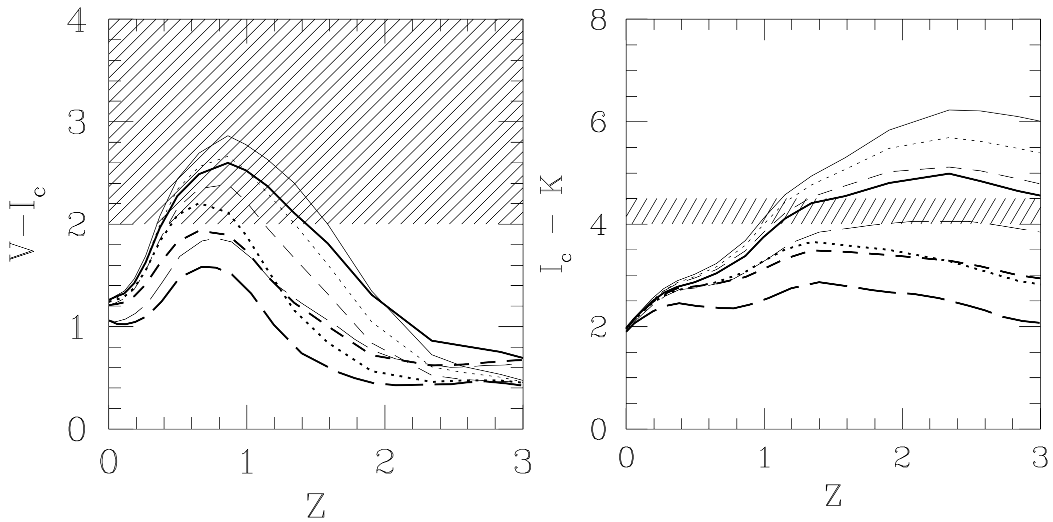

Fig. 4. $V - I_c$ and $I_c - K$ colour indices as a function of redshift for various galaxy models from Fioc and Rocca-Volmerange (1997). Bold curves are computed with evolution; thin curves without evolution (passive K-correction). Solid lines are for elliptical, dots for spiral S0, short dashes for Sa and long dashes for Sc galaxies. The zones in grey correspond to the acceptable ranges for the observed indices of the lensing galaxy G (cf. Table 3); their intersections with the curves define the redshift ranges discussed in the text.

Including in our computations galactic evolution from the lookback times to present epoch (models of Fioc and Rocca-Volmerange 1997), we find that a local elliptical galaxy with $M_K(z = 0) = -26.75$ (i.e. with a corresponding luminosity $\mathcal{L} = 4.6\mathcal{L}^*$) would produce the observed flux $K = 16.5$, if it was located at the assumed lens redshift $z = 1.32$. The proportion of known galaxies brighter than $M_K = -26.75$ is of the order of 1/1000 (Mobasher et al. 1993). The estimated luminosity would even be larger for a spiral or irregular galaxy. Making use of the Faber-Jackson (1976) relation, with $\sigma^* = 225$ km/s, the velocity dispersion of the galaxy is expected to be $\sigma = 330$ km/s. However, this empirical relation is known to be inaccurate, especially for very bright galaxies. As already mentioned, it is not possible to determine realistic values for the effective radius and surface brightness of the de Vaucouleurs profile from our data. This precludes the use of the correlation, as given by the Kormendy relation (Capaccioli et al. 1992), between the luminosity of bright elliptical galaxies and those parameters.

7 Modeling of the deflector

We have searched for a deflector model compatible with the relative positions of the QSO images A, B, and the galaxy G and also with the macrolens flux ratio of 2.8 observed between A and B. This value is derived from the emission line flux ratio (Wisotzki et al. 1995). We fix the redshift of the source at $z_{\rm s} = 2.303$ and the redshift of the deflector at $z_{\rm d} = 1.32$.

For a singular isothermal sphere (SIS) lens model, the component nearest to the galaxy ought to be the faintest, contrary to what is observed for HE 1104−1805 A and B. Indeed, with the SIS lens model, the flux ratio $(f_{\rm A}/f_{\rm B})_{\rm sis}$ between A and B is equal to 1/1.9, i.e. a factor 5 smaller than the observed macrolens flux ratio $f_{\rm A}/f_{\rm B} = 2.8$.

Therefore, we investigate the case of a SIS lens model with an additional external shear. This shear can be caused by the presence of other galaxies in the field or by the influence of undetected matter between the QSO and the observer. If we ignore the small misalignment between A, B, and G, we find a simple solution with a moderate value of the shear $\gamma = 0.121$ and with shear orientation along the A–B direction at a position angle $\phi = 114\overset{\circ}{.}6$ (see Figure 5). With $\gamma = 0.123$ and $\phi = 111\overset{\circ}{.}4$, we can even reproduce the observed slight misalignment between A, B, and G. The shear produced by a "remote" massive object has its orientation perpendicular to the direction to this object. The galaxies G1–2, roughly at position angle $\approx 320°$, are not located at a suitable position to produce the shear in the expected direction; G4–5 are better candidates. For the latter solution, the magnifications are found to be $\mu_{\rm A} = 7.02$ and $\mu_{\rm B} = 2.51$ (leading to the observed macrolens flux ratio $f_{\rm A}/f_{\rm B}$) and the time delay Δt amounts to $1.9 \times h_{50}^{-1}$ years with B leading, where $h_{50} = H_0/(50 \text{ km s}^{-1} \text{ Mpc}^{-1})$. By comparison with the simple SIS lens model which only reproduces $\theta_{\rm A}$ and $\theta_{\rm B}$ but not the flux ratio, the external shear helps to converge the light rays: the required velocity dispersion changes from $\sigma = 484$ km/s ($\gamma = 0$) to $\sigma = 454$ km/s ($\gamma = 0.123$). These values are greater than the estimates based upon the Faber-Jackson relation. This apparent discrepancy is not unexpected as the galaxy has been found to be very bright (see end of Section 6). Assuming that the lens is at $z = 1.32$, this luminous galaxy could possibly be associated with a cluster of galaxies. The extra convergence induced by such a cluster might help to reduce the amount of deflection by the galaxy itself and, hence, to lower its derived velocity dispersion. Also, if we relax the hypothesis that the lens redshift is associated with one of the absorption systems, a redshift value within the range $0.95 < z < 1.32$ is favoured as the derived absolute luminosity and velocity dispersion would be smaller.

We also tried to model the configuration with various axial symmetric lenses

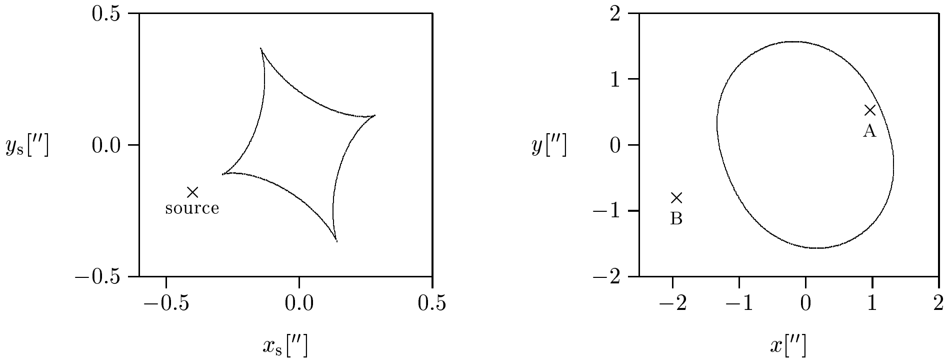

Fig. 5. Caustic with source position in the source plane (left) and critical curve with lensed image positions in the deflector plane (right). The lens is modeled as a Singular Isothermal Sphere plus external shear ($\gamma = 0.123$, $\phi = 111.4$ deg) (see text). North is up and East is to the left. The galaxy is located at the origin. The source lies at $\Delta\alpha = 0\farcs401$ and $\Delta\delta = -0\farcs179$ with respect to the galaxy (at an angular separation $\theta_s = 0\farcs439$ from the galaxy), leading to the formation of a lensed image (A) rather close to the critical line.

without external shear. With a softened power law sphere (Grogin and Narayan 1996), we only find solutions which fit the observations if we add a point mass of the order of $10^{10}\mathcal{M}_\odot$ at the center. However, all these solutions produce very high magnifications ($\mu > 100$), large core radii ($r_c > 3$ kpc) and time delays of typically half a year.

If the redshift of the deflector z_d is 1.66, the time delays are a factor 1.92 larger for all models. If $\Omega_0 = 0$ ($z_d = 1.32$), the time delay is a factor 1.35 larger than with $\Omega_0 = 1$, and if $\Omega_0 = 0.1$ it is a factor 1.30 larger. A measurement of the time delay for this system will better constrain the modeling, for a fixed value of H_0.

Since it is not difficult to reproduce the few observational constraints presently available with several plausible theoretical models, it is unlikely that a very precise value for H_o could be soon derived from the study of this system. At the moment, it is impossible to specify the likely influence of other galaxies with the help of a multiple lens model, as their masses and redshifts remain unknown. Of course, we cannot exclude that future observations of HE 1104−1805 at additional wavelengths (eg. sub-mm or X-ray) could possibly add new constraints on the model and enable one to derive H_o from time delay measurements.

As the velocity dispersion is deeply rooted in the SIS lens model, it is more convincing to investigate the likelihood of our scenario with the help of a parameter which is more robust (less model dependent). The projected mass of the deflector inside the Einstein ring, evaluated at $z = 1.32$, is:

$$\mathcal{M} = (1-\gamma)\frac{c^2}{4G}\frac{D_{\rm od}D_{\rm os}}{D_{\rm ds}}\left(\frac{\Delta\theta}{2}\right)^2 h_{50}^{-1} = 2\times 10^{12} h_{50}^{-1}\,\mathcal{M}_\odot,$$

where the angular-diameter distances D_{ij} are derived for the Einstein-de Sitter cosmological model. Adopting the solar absolute magnitude $M_{V\odot} = 4.83$, $M_K(z=0) = -26.75$ and $V-K(z=0) = 3.23$ (see Figure 4 and Section 6), we derive a mass-to-light ratio $\mathcal{M}/\mathcal{L} = 11\,h_{50}\,\mathcal{M}_\odot/\mathcal{L}_\odot$. We have also computed the mass-to-light ratio as a function of the lens redshift. It decreases from $18\,h_{50}\,\mathcal{M}_\odot/\mathcal{L}_\odot$ at $z_{\rm d} = 0.5$ to $10\,h_{50}\,\mathcal{M}_\odot/\mathcal{L}_\odot$ at $z_{\rm d} = 2.3$. Although very bright and very massive, the lens would have a derived mass-to-light ratio similar to those of known elliptical lensing galaxies (Kochanek 1995, Léhar 1993). The claim that the galaxy would be a dark lens with $\mathcal{M}/\mathcal{L} > 540\mathcal{M}_\odot/\mathcal{L}_\odot$ by Hawkins (1997) is based on the hypothesis, that $z_{\rm d} = 0.5$ and $R > 24$. Our present study excludes such a possibility.

8 Conclusions

This paper reports our direct imaging efforts and some theoretical investigations in order to better understand the physical nature of the doubly imaged quasar HE 1104−1805.

The detection of a very red galaxy located between the two components of HE 1104−1805 proves the validity of the gravitational lensing hypothesis to explain this interesting object. The claim that a microlensing event is occurring for image A, proposed to explain the colour differences between A and B (Wisotzki et al. 1993, 1995), is supported by our analysis.

From our derivation of the IR and optical magnitudes, the lens is most likely found to be an elliptical galaxy with redshift $0.95 < z < 1.4$. This leads to a coherent scenario in which one can also explain the two main absorption line systems observed in the spectra of the quasar components. The $z = 1.32$ absorption is produced in the spectra of A and B by the deflector (a bright elliptical with $\mathcal{L} \approx 4.6\mathcal{L}^*$). This galaxy would presently be the most distant known gravitational lens forming a QSO mirage. The hypothesis of a lensing galaxy at $z = 1.66$ is poorly supported by the present observations. The $z = 1.66$ absorption system is likely induced by absorbing gas in a foreground, yet unrevealed, disk galaxy. However, it might well be that the redshift of the lens is not associated with any of the absorption line systems. In such a case, redshift values for the lens within the range $0.95 < z < 1.32$ would be favoured.

A singular isothermal sphere lens model located at $z = 1.32$ with an additional shear term of 0.123 can easily explain the observed QSO images positions and the flux ratio between A and B. The physical origin of the additional shear is unknown. It may originate in an asymmetry of the galaxy gravitational potential, in the combined effect of several foreground galaxies located near the projected position of the quasar (see Figure 1) and/or of a possible galaxy cluster associated with the main lens.

The galaxy is found to be very massive ($2\times10^{12} h_{50}^{-1} \mathcal{M}_{\odot}$). Its mass-to-light ratio does not much depend on the redshift within the range $0.95 < z < 1.4$. For a deflector at $z = 1.32$, this ratio is estimated to be $\mathcal{M}/\mathcal{L} \sim 11\, h_{50}\, \mathcal{M}_{\odot}/\mathcal{L}_{\odot}$; the proportion of dark to luminous matter for this galaxy is fully compatible with what is observed for other known lensing elliptical galaxies.

With the help of the ground-based and HST optical data, we have also reported a possible photometric variability for the quasar by about 0.28 mag (A) and 0.15 mag (B) in V and I_c on a time scale of 2 years. This last result (together with the simple modeling described above) stresses the need for a sustained spectroscopic and photometric monitoring campaign of HE 1104−1805.

Acknowledgments

Part of this work has been supported by the SSTC/PRODEX project (HST observations of gravitational lenses) and a Belgian FNRS grant (travel support for JS). We thank Patrick Petitjean for providing us with some useful information on optical counterparts of known damped Lyα and metallic absorption line systems. We also wish to thank the anonymous referee for his very constructive remarks.

FG acknowledges support from the Danish Natural Science Research Council (SNF) and thanks Peter Stetson for letting him use ALLFRAME for this project.

SR would like to acknowledge D. Reimers and S. Lopez for interesting discussions and R. Quast for some calculations.

References

[1] Caon, N., Macchetto, F., Pastoriza, M.G., 1995, BAAS 27 (4), 1407

[2] Capacciola, M., Caon, N., D'Onofrio, M., 1992, MNRAS, 259, 323

[3] Dunlop, J., Peacock, J., Spinrad, H., Dey, A., Jimenez, R., Stern, D., Windhorst, R., 1996, Nature, 381, 581

[4] Faber, S.M., Jackson, R.E., 1976, ApJ, 204, 668

[5] Fioc, M., Rocca-Volmerange, B., 1997, AA, 326, 950

[6] Freudling, W., 1995, PASP 107, 85

[7] Fruchter, A., 1997, to appear in the Proceedings of the "1997 HST Calibration Workshop", Casertano et al. (eds)

[8] Grogin, N. A., Narayan, R., 1996, ApJ, 464, 92

[9] Grundahl, F., Hjorth, J., Sørensen, A.N., 1995, Highlights of Astronomy, 10, 658

[10] Hawkins, M.R.S., 1997, accepted for publication in AA

[11] Holtzmann, J.A., Burrows, C.J., Casertano, S., Hester, J.J., Trauger, J.T., Watson, A.M., Worthey, G., 1995, PAPS 107, 1065

[12] Hook, R., Lucy, L., 1994, in "The restoration of HST images and spectra — II", Hanish, R., White, R. (eds.), 86

[13] Kochanek, C.S., 1995, ApJ, 445, 559

[14] Krist, J., Hook, R., 1996, available on the WWW (http://scivax.stsci.edu/ krist/tinytim.html)

[15] Krist, J., 1997, Postscript document available on the WWW (http://www.stsci.edu/ftp/instrument_news/WFPC2/Wfpc2_serv/wfpc2_ghosts.ps)

[16] Le Brun, V., Bergeron, J., Boissé, P., Deharveng, J.M., 1997, AA 321, 733

[17] Léhar, J., Langston, G.I., Silber, A., Lawrence, C.R., Burke, B.F., 1993, AJ, 105, 847

[18] Lopez, S., Reimers, D., Smette, A., 1998, in preparation

[19] Mobasher, B., Sharple, R.M., Ellis, R.S., 1993, MNRAS, 263, 560

[20] Østensen, R., Remy, M., Lindblad, P.O. et al., 1997, AA Suppl., in press

[21] Plana, H., Boulesteix, J., 1996, AA 321, 733

[22] Smette, A., Robertson, J.G., Shaver, P.A., Reimers, D., Wisotzki, L., Köhler, T., 1995, AA Suppl., 113, 199

[23] Stetson, P. B., 1987, PASP, 99, 191

[24] Stetson, P. B., 1994, PASP, 106, 250

[25] Walsh, D., Carswell, R.F., Weymann, R.J., 1979, Nature, 279, 381

[26] Whitmore, B., 1997, PostScript document available on the WWW (http://www.stsci.edu/ftp/instrument_news/WFPC2/Wfpc2_phot/photom2.ps)

[27] Wisotzki, L., Köhler, T., Kayser, R., Reimers, D., 1993, AA, 278, L15

[28] Wisotzki, L., Köhler, T., Ikonoumou, M., Reimers, D., 1995, AA, 297, L59